Study of WO3-decorated porous silicon and Al2O3-ALD encapsulation

R. Benabderrahmane Zaghouani, M. Alaya, H. Nouri, J.-L. Lazzari, W. Dimassi

Study of WO3-decorated porous silicon and Al2O3-ALD encapsulation

R. Benabderrahmane Zaghouani, M. Alaya, H. Nouri, J.-L. Lazzari, W. Dimassi

Study of WO_3-decorated porous silicon and Al_2O_3-ALD encapsulation

R. Benabderrahmane Zaghouani[1] · M. Alaya[1] · H. Nouri[1] · J.-L. Lazzari[2] · W. Dimassi[1]

Received: 11 July 2018 / Accepted: 14 August 2018

Abstract

In this work, we report on the encapsulation of WO_3-decorated porous silicon aluminum oxide (Al_2O_3). Porous layers, elaborated for different current densities, are decorated by quasi-spherical WO_3 nanoparticles with different densities and sizes. AFM analysis shows that the WO_3 deposition is controlled by the prepared porous silicon morphology. WO_3-treated porous silicon samples were faithfully coated by ALD-Al_2O_3. A significant enhancement of porous silicon reflectance after AL_2O_3/WO_3 deposition was obtained. In order to quantify the passivation effect of the dual treatment, the effective diffusion length (L_{eff}) of the minority carriers is determined by Light Beam Induced Current (LBIC) measurements. An increase of L_{eff} from 74 µm in porous silicon to 532 µm in AL_2O_3/WO_3/PS sample is reached. This enhancement is attributed to the dangling bonds saturation by alumina and tungsten oxide which leads to the diminution of the surface recombination velocities.

1 Introduction

Since its discovery [1], porous silicon (PS) is considered as an interesting material in different fields such as microelectronics, optical, photovoltaic, and sensing applications thanks to its properties: low surface reflection, high visible photoluminescence, and high internal surface [2–5]. To be integrated in solar cells, silicon nanostructures such as silicon nanowires [5] and PS, with their unstable surface in ambient conditions, should be passivated in order to ameliorate their optoelectronic properties. In particular, the minority carrier lifetime, a key parameter in silicon-based solar cells, is degraded in PS. In our previous work [6], we have reported on the passivation of PS, elaborated by stain-etching method, by tungsten oxide (WO_3). An enhancement of the photoluminescence of WO_3-treated porous silicon (WO_3/PS) is obtained. Moreover, the elaborated samples had a low surface reflectance up to about 5%. An enhancement of the minority carrier lifetime was obtained thanks to surface recombination velocity decrease by saturating the dangling bonds by WO_3. Obtained results have confirmed that tungsten oxide is a good passivation layer to improve PS properties. In addition to that, the morphological results have shown that WO_3 is deposited in the form of nanoparticles without covering the total surface of PS. To achieve a maximum of enhancement, the PS surface should be totally protected to reduce the surface recombination velocity. This could be achieved by depositing a passivating thin layer. In fact, the traditional passivation schemes used in photovoltaics are silicon dioxide (SiO_2), hydrogenated amorphous silicon nitride (a-SiNx:H) and hydrogenated amorphous silicon (a-Si:H) [7, 8]. These materials provide good passivation levels but present some limits such as the low passivation of highly doped p-type silicon in the case of a-SiNx:H, the high processing temperature for the SiO_2, the significant absorption in the visible and the thermal instability for the a-Si:H and the a-SiNx:H [9, 10]. Many research reports have demonstrated that Al_2O_3 films provide an excellent passivation of both n and p type silicon [9] thanks to the combination of two mechanisms: the filed-effect passivation thanks to the presence of a high negative fixed charge density at the interface with silicon and the chemical passivation by reducing the interface state density. Another interesting issue is that Al_2O_3 has a large bandgap so it acts as an optical window leading to no significant absorption of the visible light which is very important in solar cells. Different deposition schemes are reported in the literature to obtain aluminum oxide such as pyrolysis [11], sol–gel [12], plasma enhanced chemical vapor deposition using the trimethyl aluminum (TMA) [13, 14], sputtering [15], atomic layer deposition (ALD) using TMA as a precursor [16].

✉ R. Benabderrahmane Zaghouani
rabia.benabderrahmane@gmail.com

1 Laboratoire de Photovoltaïque, Centre de Recherches et des Technologies de l'Energie, Technopôle de Borj-Cédria, BP, 95 Hammam-Lif, Tunis, Tunisia

2 Aix Marseille Université, CNRS, CINaM UMR 7325, Campus de Luminy, Case 913, 163, Avenue de Luminy, 13288 Marseille Cedex 09, France

Interestingly, the alumina thin films deposited by ALD could permit the uniform coating of nanostructures, in particular PS.

In this work, we report on the encapsulation of WO_3/PS by alumina grown by ALD. The Al_2O_3/WO_3/PS structures performance is investigated by analyzing reflectance, current–voltage response and effective diffusion length measurement using the Light Beam Induced Current (LBIC) technique.

2 Experimental techniques

2.1 Materials preparation

PS samples were elaborated by electrochemical etching of polished P^+ type silicon wafer, (100) orientation, boron doped with a resistivity of 0.01–0.02 Ω cm and a thickness of 450 µm in a mixture of hydrofluoric acid (40%) and absolute ethanol in the volume ratio of (1:4) with different current densities (5, 10, 15, 20 and 25 mA/cm^2) during 10 min. Before PS elaboration, silicon substrates were cleaned with boiling acetone for 10 min, followed by immersion in ethanol for 5 min and rinsed after that in deionized water in order to eliminate organic greases. Finally, the substrates were etched in 10% hydrofluoric acid for 1 min to eliminate native oxide, rinsed in deionized water and dried with nitrogen flux. In order to obtain homogeneous PS films, an aluminum layer with a thickness of 300 nm was deposited on the back side of the silicon wafer by thermal evaporation followed by annealing under vacuum at 300 °C during 20 min. After PS formation, the samples were dip-coated during 360 s in a solution of a concentration 0.018 mol/L containing tungsten hexachloride (WCl_6) prepared previously in order to deposit WO_3 layers [6, 17]. WO_3/PS samples were then coated by aluminum oxide layer of a thickness of 50 nm grown by ALD technique using TMA and H_2O as precursors at a temperature of 100 °C. The deposition parameters are listed in Table 1.

2.2 Characterization tools

The morphological features of the different prepared samples were characterized by a Digital Instruments Nanoscope III atomic force microscopy (AFM) operating in tapping mode and a scanning electron microscope (SEM) JEOL JSM-6340F. The optical properties of the samples based on the surface reflectance were analyzed using PerkinElmer Lambda 950 UV/VIS. The effect of the dual treatment (Al_2O_3/WO_3) on PS electrical properties is studied by LBIC measurements performed on a home-made set-up [18].

Table 1 ALD processing parameters

ALD parameters	TMA	N_2	H_2O	N_2	T
	0.1 s	3 s	0.1 s	4 s	100 °C

3 Results and discussion

3.1 Investigation of WO_3 deposition by AFM

PS samples are elaborated under different current densities during 10 min. The porosity and the thickness of the etched layers are determined by gravimetric measurements and are presented in Fig. 1. Figure 2 shows the AFM images for PS and WO_3/PS samples prepared for the different etching current densities. In order to deposit WO_3, the different PS samples are immersed in the WCl_6 solution for the same duration. As we can see, the PS surface for all samples is covered by quasi-spherical nanoparticles with different densities and sizes. This observation shows that the WO_3 deposition is controlled by the prepared PS morphology. This result is confirmed by the RMS values recapitulated in Table 2. The PS measured RMS varies from 0.17 to 0.35 nm. These low RMS values are attributed to the electrochemical etching technique used which offers a good surface homogeneity in the contrary to the stain etching technique [19]. After WO_3 deposition, the RMS is changing from 0.54 to 9.58 nm for anodization current density of 5 and 25 mA/cm^2 respectively. Moreover, the ratio RMS (PS)/RMS (WO_3/PS) is varying from 1.54 to 39.08. All these observations confirm the control of the WO_3 nanoparticles properties by modifying the PS parameters.

3.2 Encapsulation of WO_3/PS structures by ALD-Al_2O_3

As shown in [6], the tungsten oxide has improved the PS electronic and optical properties. A further amelioration of the deposited films properties can be reached by the deposition of alumina as it coats the total surface of the nanostructured surface. In particular, the reduction of the surface recombination velocity can be obtained. In addition to

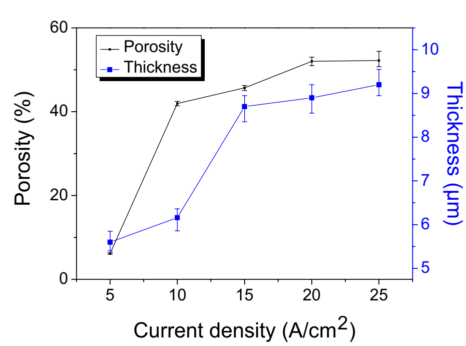

Fig. 1 The evolution of the PS porosity and thickness with the etching current density

that, alumina can protect these structures from atmospheric degradation.

Figure 3 shows the top-view SEM image of the PS surface elaborated with a current density of 20 mA/cm^2. The pores, perfectly circular, are uniformly formed on the surface. After immersion in the prepared WCl_6 solution during 360 s, PS surface was covered with quasi-spherical WO_3 nanoparticles (Fig. 4). The formed nanostructures have an average size of 60 nm. Then, Al_2O_3 layer with 50 nm of thickness is deposited on WO_3/PS sample (Fig. 5). As shown in Fig. 5, the WO_3 nanoparticles are faithfully coated with alumina. The roughness evolution with the different treatments is determined by AFM micrographs of PS, WO_3/PS and Al_2O_3/WO_3/PS samples. After WO_3 deposition, the RMS is increased from 0.24 nm for PS sample to 9.38 nm for WO_3/PS and when depositing aluminum oxide, the RMS is decreased to about 6 nm due to the pores filling by alumina.

3.3 Surface reflectance analysis

PS is considered as an efficient antireflection layer that could be integrated in photovoltaic applications thanks to the light-trapping into the pores. The elaborated structures based on PS should keep or better ameliorate the antireflection aspect of the porous layer. In Fig. 6, we compare the surface reflectance of PS and Al_2O_3/WO_3/PS samples. The spectra show a significant enhancement of PS reflectance after the different treatments. The reflectance decreases from about 25% for PS sample to about 12% for Al_2O_3/WO_3/PS sample in the visible region. This result is attributed to the combined effect of both WO_3 nanostructures and aluminum oxide. As demonstrated in [6], the WO_3 integration leads to PS reflectance decrease. The obtained low reflectance, in particular around the visible region of the solar spectrum, is encouraging the integration of these structures in an efficient photovoltaic device.

3.4 Current–voltage analysis

To investigate the efficiency of the different treatment, current–voltage analysis was carried on. Figure 7 shows the I–V characteristic of the elaborated diodes, Al/PS and Al/Al_2O_3/WO_3/PS, measured at room temperature under dark conditions. After PS treatment with tungsten oxide and alumina, an increase in the current is obtained. Moreover, the threshold voltage from which a noticeable current increase is shifted to lower value in the case of the Al/Al_2O_3/WO_3/PS diode attributed to the conduction amelioration.

3.5 LBIC analysis

The formation mechanism of PS leads to H-terminated surface which is unstable in ambient conditions. Due to the appearance of dangling bonds on PS surface the effective minority carrier lifetime (τ_{eff}) is deteriorated. In fact, τ_{eff} takes into account the lifetime in the bulk and at the surface as depicted in Eq. (1).

$$\frac{1}{\tau_{eff}} = \frac{1}{\tau_{bulk}} + \frac{1}{\tau_{surface}} \tag{1}$$

The surface lifetime, related to the surface recombination velocity, could be ameliorated by passivating the surface leading to the enhancement of the effective diffusion length (L_{eff}) which is related to τ_{eff} by the following equation:

$$L_{eff} = \sqrt{D \times \tau_{eff}} \tag{2}$$

where D is the diffusion coefficient.

L_{eff} gives an evaluation of the quality of the structure as it depends on the bulk diffusion length (L_b) and the effective surface recombination velocities (S_{eff}).

As mentioned above, in our previous work [6], the PS surface coating by WO_3 has ameliorated the effective minority carrier lifetime by decreasing the surface recombination velocity which could be enhanced by alumina coating. In order to quantify the effect of the Al_2O_3 encapsulation on the electronic properties of the WO_3/PS, the diffusion length of the minority carriers is determined by LBIC measurements. LBIC is based on the scanning of the sample surface by a light beam leading to the creation of electron–holes pairs. The collected current is depending L_{eff} which is affected by the scanned surface quality. In our experiment, the laser diode with a wavelength $\lambda = 632$ nm is focused perpendicular to the sample surface leading to a penetration depth around 3 µm in silicon. The carrier's generation is then occurring in the PS. Figure 8 presents the measured current I_{LBIC} as a function of the beam position (x) for the Al_2O_3/WO_3/PS sample and the untreated PS. In order to determine L_{diff}, the current decay is fitted using the following theoretical expression Eq. (3) [20]:

$$I \alpha \exp\left(-\frac{x}{L_{eff}}\right) + I_0 \tag{3}$$

An effective diffusion length of 74 µm is obtained for the PS sample. The coating of the PS sample by Al_2O_3/WO_3 layers has increased the diffusion length to about 532 µm. This enhancement is attributed to the dangling bonds saturation by alumina and tungsten oxide which leads to the diminution of the surface recombination velocities. This result is confirming the passivation effectiveness of PS by the Al_2O_3/WO_3 dual treatment.

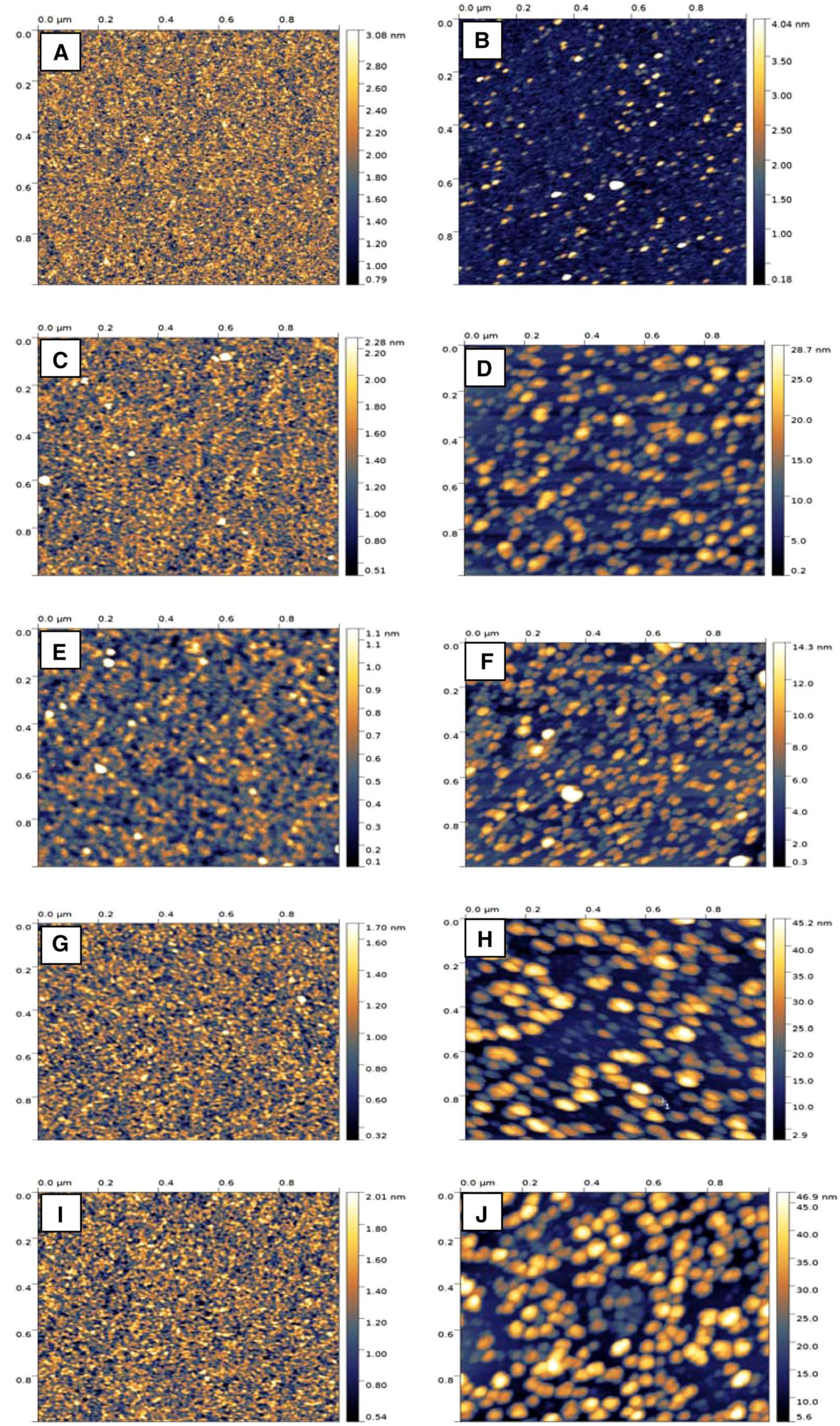

A
3.08 nm
B
4.04 nm
C
2.28 nm
D
28.7 nm
E
1.1 nm
F
14.3 nm
G
1.70 nm
H
45.2 nm
I
2.01 nm
J
46.9 nm

◂**Fig. 2** AFM images of PS and WO_3/PS samples elaborated at different etching current densities: **a, b** 5 mA/cm^2, **c, d** 10 mA/cm^2, **e, f** 15 mA/cm^2, **g, h** 20 mA/cm^2, **i, j** 25 mA/cm^2

Table 2 Measured RMS for PS and WO_3/PS for different electrochemical etching current density

Current density (mA/cm^2)	5	10	15	20	25
RMS (PS) (nm)	0.35	0.33	0.17	0.24	0.28
RMS (WO_3/PS) (nm)	0.54	4.66	2.49	9.38	9.58
RMS (PS)/RMS (WO_3/PS)	1.54	14.12	14.64	39.08	34.21

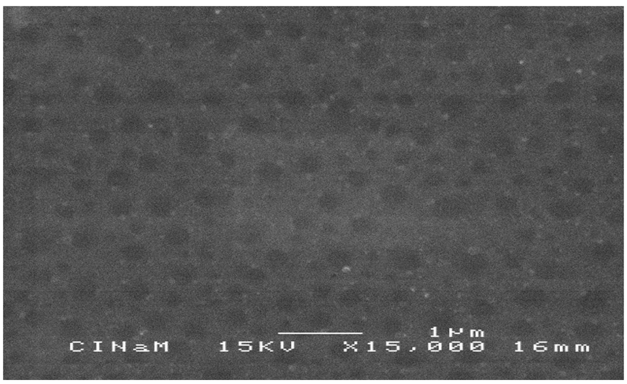

Fig. 3 Top surface SEM view of PS surface

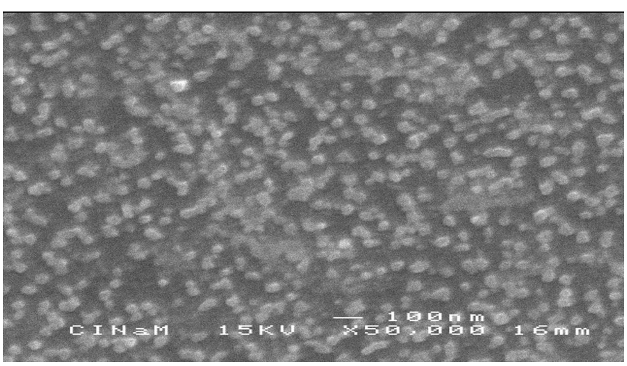

Fig. 4 Top surface SEM view of PS surface covered with WO_3 nanoparticles

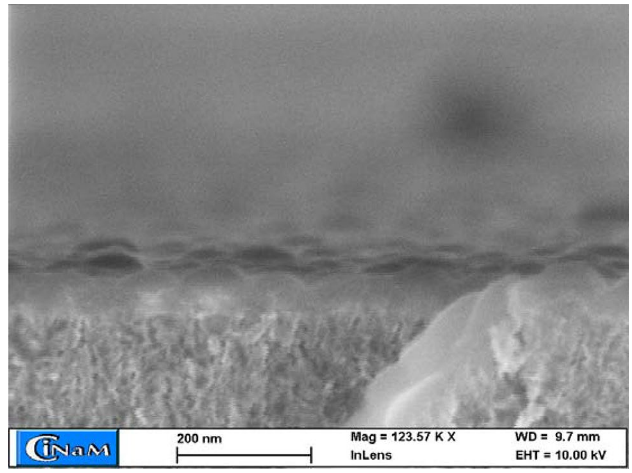

Fig. 5 Cross-section SEM image of Al_2O_3/WO_3/PS sample

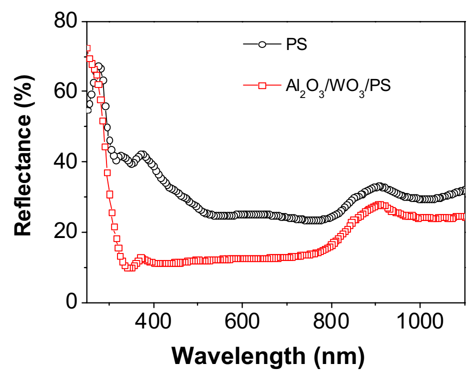

Fig. 6 Reflectance spectra of PS and Al_2O_3/WO_3/PS samples

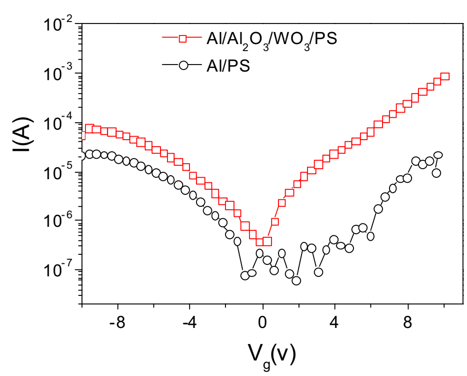

Fig. 7 Current versus applied voltage Vg for Al/PS and Al/Al_2O_3/WO_3/PS diodes

4 Conclusion

In this study, we have evaluated the effects of tungsten oxide and alumina treatment on PS optoelectronic properties. AFM confirmed the total coverage of PS surface by WO_3 nanostructured thin film. The density and the size of the deposited WO_3 nanoparticles are controlled by the PS morphology. These structures are faithfully coated by an encapsulation by Al_2O_3 layer. We have demonstrated that the dual treatment Al_2O_3/WO_3 has improved the PS reflectance. Moreover, the PS passivation is confirmed by the enhancement of the minority carrier diffusion length which increases from 74 μm for the untreated sample to 532 μm for the

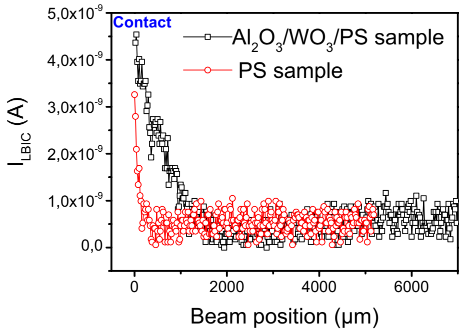

Fig. 8 Experimental LBIC profiles for PS and $Al_2O_3/WO_3/PS$ samples

treated one. These interesting results encourage the integration of these structures in different optoelectronic devices.

Acknowledgements The authors wish to thank Alain Ranguis and Damien Chaudanson for AFM and SEM measurements done at the *Centre Interdisciplinaire de Nanoscience de Marseille* (CINaM).

References

1. L.T. Canham, Appl. Phys. Lett. **57**, 1046 (1990)
2. R.T. Collins, P.M. Fauchet, M.A. Tischler, Phys. Today **50**, 24 (1997)
3. A. Richter, P. Steiner, F. Kozlowski, W. Lang, IEEE Electron Devices Lett. **12**, 691 (1991)
4. M. Rajabi, R.S. Dariani, J Porous Mater. **16**, 513 (2009)
5. M.Y. Tabassi, R.B. Zaghouani, M. Khelil, K. Khirouni, W. Dimassi, J. Mater. Sci.: Mater. Electron. **28**, 9717 (2017)
6. M. Alaya, R.B. Zaghouani, S. Khamlich, J.L. Lazzari, W. Dimassi, Thin Solid Films **645**, 51 (2018)
7. A.G. Aberle, Sol. Energy Mater. Sol. Cells **65**, 239 (2001)
8. S. Dauwe, J. Schmidt, R. Hezel, In *29th IEEE Photovoltaic Specialists Conference*, New Orleans (2002)
9. B. Hoex, S.B.S. Heil, E. Langereis, M.C.M. Van de Sanden, W.M.M. Kessels, Appl. Phys. Lett. **89**, 042112 (2006)
10. S. Dauwe, L. Mittelstädt, A. Metz, R. Hezel, Prog. Photovolt. Res. Appl. **10**, 271 (2002)
11. R. Hezel, K. Jaeger, J. Electrochem. Soc. **136**, 518 (1989)
12. P. Vitanov, A. Harizanova, T. Ivanova, T. Dimitrova, Thin Solid Films **517**, 6327 (2009)
13. G. Dingemans, M.C.M. Van de Sanden, W.M.M. Kessels, Electrochem. Solid-State Lett. **13**, H76 (2010)
14. P. Saint-Cast, J. Benick, D. Kania, L. Weiss, M. Hofmann, J. Rentsch, R. Preu, S.W. Glunz, IEEE Electron Device Lett. **31**, 695 (2010)
15. T.T. Li, A. Cuevas, Phys. Status Solidi (RRL)-Rapid Res. Lett. **3**, 160 (2009)
16. G. Dingemans, N.M. Terlinden, D. Pierreux, H.B. Profijt, M.C.M. Van de Sanden, W.M.M. Kessels, Electrochem. Solid-State Lett. **14**, H1 (2011)
17. S. Badilescu, P.V. Ashrit, Solid State Ion. **158**, 187 (2002)
18. M.B. Rabha, W. Dimassi, M. Bouaïcha, H. Ezzaouia, B. Bessais, Sol. Energy **83**, 721 (2009)
19. M.B. Rabha, M. Salem, M.A. El Khakani, B. Bessais, M. Gaidi, Mater. Sci. Eng. B **178**, 695 (2013)
20. Y. Sayad, A. Kaminski, D. Blanc, A. Nouiri, M. Lemiti, Superlatt. Microstruct. **45**, 393 (2009)